ADVANCED OPTICAL MATERIALS
www.advopticalmat.de

Rational Design of Mechano-Responsive Optical Materials by Fine Tuning the Evolution of Strain-Dependent Wrinkling Patterns

Philseok Kim, Yuhang Hu, Jack Alvarenga, Mathias Kolle, Zhigang Suo, and Joanna Aizenberg**

Rational design strategies for mechano-responsive optical material systems are created by introducing a simple experimental system that can continuously vary the state of bi-axial stress to induce various wrinkling patterns, including stripes, labyrinths, herringbones, and rarely observed checkerboards, that can dynamically tune the optical properties. In particular, a switching of two orthogonally oriented stripe wrinkle patterns from oxidized polydimethylsiloxane around the critical strain value is reported, as well as the coexistence of these wrinkles forming elusive checkerboard patterns, which are predicted only in previous simulations. These strain-induced wrinkle patterns give rise to dynamic changes in optical transmittance and diffraction patterns. A theoretical description of the observed pattern formation is presented which accounts for the residual stress in the membrane and allows for the fine-tuning of the window of switching of the orthogonal wrinkles. Applications of wrinkle-induced changes in optical properties are demonstrated, including a mechanically responsive instantaneous privacy screen and a transparent sheet that reversibly reveals a message or graphic and dynamically switches the transmittance when stretched and released.

1. Introduction

Wrinkles can form when a membrane experiences a large compressive stress due to differential growth of tissue, thermal stress, solvent-induced swelling, or mechanical compression.[1–5] They exist over a wide range of length scales, from rippled cloths and papers, the epidermis of aging human skin and pruney fingers after a long bath, dehydrated leathery plant leaves, to a graphene sheet under a compressive load.[4,6] Biological systems cleverly utilize wrinkle patterns on their skin to create intriguing optical effects, such as the iridescent colors found on the elytra of various beetles (e.g. cuticular grating of Sphaeridiinae (Hydrophilidae))[7] and on the petals of flowers (e.g. epidermal cells of Queen of the Night tulips),[8] and dynamically changing camouflaged various shapes and textures of the skin of cephalopods[9] to attract their mates and pollinators, to lure their prey, or to deceive their predators. Likewise, controlled and reversible wrinkled surfaces may provide an important concept in materials design, but the precise control and understanding of the conditions to generate desired wrinkle patterns with high level of complexity is still largely missing. Theoretical studies predict various patterns generated by buckling of a thin membrane in response to a bi-axial stress, such as stripes (a periodic array of straight wrinkles), labyrinths (disordered zigzag wrinkles), herringbones (a periodic array of zigzag wrinkles), and checkerboards.[2,10,11] However, in previous experimental systems, only a limited number of possible buckling patterns (e.g. stripes and herringbones) have been predominantly observed. Therefore, it is important to devise a new experimental system that can fine-tune the bi-axial stress in a thin film to create and elucidate all possible buckling patterns including some of the mysterious and rarely observed patterns and their associated optical effects.

Here we introduce an experimental system that can continuously vary the state of bi-axial stress over a wide range and allow for the creation of various wrinkling patterns. This is achieved by the interplay between the residual strain (thermal and intrinsic strain) and the applied mechanical strain (uni-axially stretching and releasing). Using a pre-stretching approach, the applied mechanical strain can be adjusted to a very small magnitude comparable to that of residual strain thereby effectively creating continuously varying conditions of very small bi-axial stresses, isotropically and anisotropically. As a result, we were able to address a very narrow range of bi-axial stresses around the critical buckling stress to investigate the strain-dependent changes in the wrinkle patterns found in oxygen plasma-treated PDMS and their optical signatures. We discuss the detailed correlations between their macroscopic optical properties and the microscopic changes in the pattern of the wrinkles under

Dr. P. Kim, J. Alvarenga, Prof. J. Aizenberg
Wyss Institute for Biologically Inspired Engineering
Harvard University
60 Oxford St., Cambridge, MA, 02138, USA
E-mail: philseok.kim@wyss.harvard.edu;
Jaiz@seas.harvard.edu
Dr. Y. Hu, Dr. M. Kolle, Prof. Z. Suo, Prof. J. Aizenberg
School of Engineering and Applied Sciences and Kavli Institute for Bionano Science and Technology
Harvard University
29 Oxford St., Cambridge, MA, 02138, USA

DOI: 10.1002/adom.201300034

a given mechanical load. In particular, we report a switching behavior of the two orthogonal stripe wrinkle patterns and diffraction patterns linked, and their coexistence near the critical strain value, resulting in the first observation of the elusive checkerboard patterns in a simple strain experiment, which were predicted only in previous simulations. A simple analytical model accounting for the residual stress in the membrane is presented that captures these new experimental observations and suggests the existence of the upper and lower bound of strain for the orthogonal wrinkle patterns to appear. We also demonstrate applications based on the dynamic optical switching behavior of the wrinkled PDMS, such as instantaneous privacy screens and reversibly appearing and disappearing messages or graphics upon stretching.

2. Results and Discussion

Polydimethylsiloxane (PDMS) is widely used in soft lithography as casting molds, microfluidic devices, substrates and components for flexible and wearable electronics and soft robotics.[12,13] The most commonly used PDMS (Sylgard 184, DOW Chemical) has the optical clarity close to that of glass and its oxidation-induced skin layer has good adhesion to the substrate. When the oxidized PDMS substrate is subject to a mechanical strain above a critical load, the stiff skin layer can buckle into a quasi-ordered array of wrinkles.[14]

We used oxygen plasma treatment as a means to create a stiff, glass-like surface layer and strain-dependent wrinkle patterns on a thermally cured PDMS (Dow Sylgard 184 with 10:1 base to hardener ratio) sheet by two methods (**Figure 1**). In a type A sample, the PDMS sheet is uni-axially pre-stretched, exposed to oxygen plasma, and then the pre-stretch is released. In a type B sample, the PDMS sheet is exposed to oxygen plasma without pre-stretch. Both types of samples develop wrinkles when the substrate is significantly deformed.

2.1. Strain-Dependent Optical Properties of Wrinkled PDMS

The quasi-ordered wrinkles diffract visible light and make the PDMS sheet iridescent and translucent. The overall effect is a reversible transition between an optically clear/transparent state and a translucent/diffusive state with some iridescence when the PDMS sheets are stretched and released. Samples prepared with pre-stretching (type A, Figure 1A) are translucent and diffusive when the pre-stretch is released, but become clear and transparent when stretched back to the initial pre-stretched shape. These samples become translucent and diffusive again when over-stretched beyond the initial pre-stretch. In contrast, samples prepared without pre-stretching (type B, Figure 1B) are clear and transparent when there is no strain, but become translucent and iridescent when stretched, due to the compression perpendicular to the axis of stretching causing wrinkle formation. In both cases, the stretching process is reversible within the limit of tensile strength of the PDMS, and the visual appearance of the oxygen plasma-treated PDMS sheet can be reversibly changed. All of these stretching-releasing processes can be repeated for an indefinite number

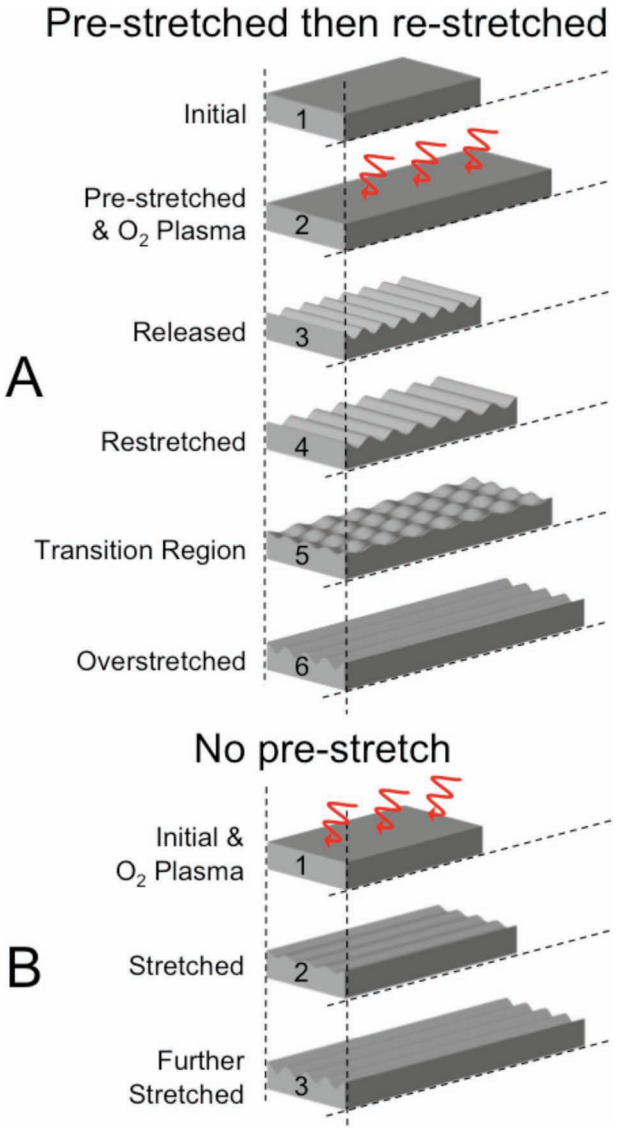

Figure 1. Schematics (not to scale) of preparation procedures for sample type A (with pre-stretching) and sample type B (without pre-stretching).

of cycles (>100 000 times at 0.5 Hz for 72 h) with no noticeable change in the apparent optical properties.

To correlate the optical properties of oxygen plasma-treated PDMS and applied strain, we characterized the optical transmittance of the samples in the visible–NIR range (400–900 nm) mounted on a custom-built stretching device. **Figure 2** shows the normal incidence optical transmittance spectra recorded for PDMS samples prepared with different pre-stretching conditions. An untreated PDMS substrate of identical thickness (1 mm) was used as a control sample where no noticeable optical signature was detected over the 400–900 nm range and as a function of applied mechanical strain (See Supporting Information Figure S1A). All samples with different pre-stretching conditions exhibited maximum transparency when stretched back to the initial pre-stretched length. This is due to the effective reduction of stress and surface topography

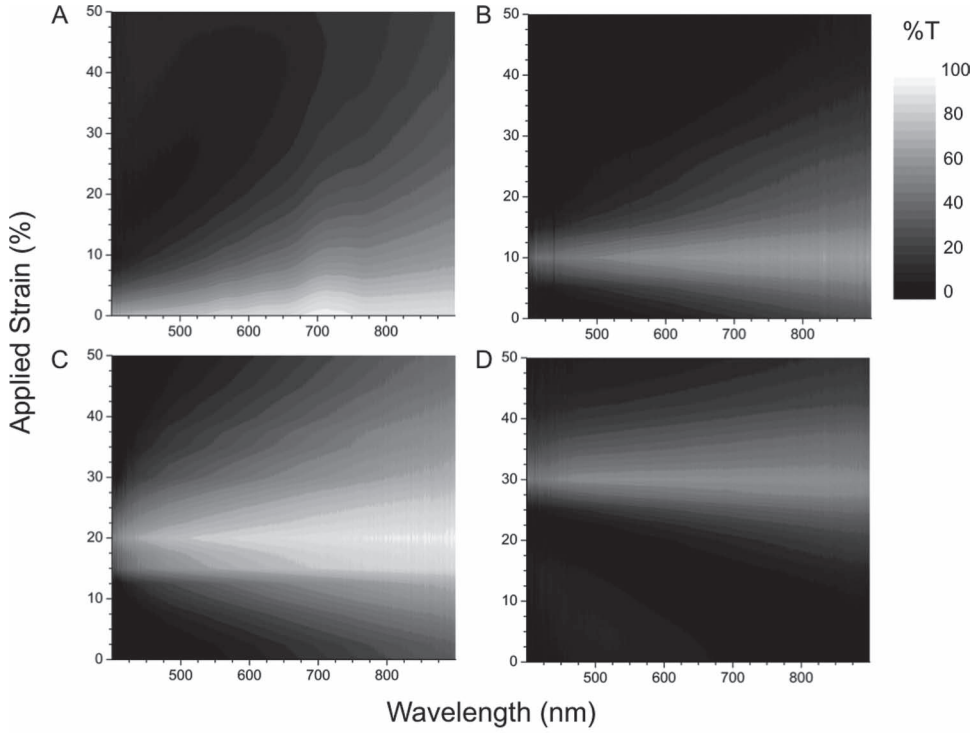

Figure 2. Optical transmittance contour plot of wrinkled PDMS sheets (thickness = 1 mm) as a function of wavelength and applied strain. A) sample type B; B–D) sample type A with pre-stretching values of 10, 20, and 30%, respectively.

in the membrane by stretching it back to its original dimension at which the oxidized layer was created by oxygen plasma treatment. For the type A samples, the transmittance values increased linearly with the applied strain until reaching a maximum value, then decreased (scaling approximately at a power of ½ of the applied strain due to the compression caused by the large Poisson's ratio of PDMS). We attribute the wavelength-dependent changes in the in-line transmittance to the variation in diffraction efficiency for specific wavelengths that is associated with the change in wrinkle amplitude (0 to ~1.2 μm change from minimum to maximum amplitude for 20% pre-stretched type A sample) and frequency (~3.7μm at 0% stretch to ~4.7 μm at 20% stretch, then ~4.3 μm at 35% stretch for 20% pre-stretched type A sample), which in this system depend on the applied strain as shown in **Figure 3**.

We also observed decrease in the 0^{th} order diffraction intensity when the sample was stretched or released away from the original pre-stretched dimensions. The decrease in the transmitted light intensity coincided with the increase in the intensity of the higher order diffracted light, which was not collected by the fiber optic detector placed in parallel with the incident light to the sample. Therefore, the main mechanism leading to the changes in the transmittance arises from the onset of the diffraction due to the onset of buckling, then subsequent increase in the diffraction efficiency of the wrinkles as the amplitude of the wrinkles increases with increased strain. When the PDMS is under a large strain, the Mie scattering effect due to cracks begins to add to the optical properties as evidenced by the diffusive lines spreading off of the diffraction spots in **Figure 4**. Therefore, the overall switching effect of macroscopic optical transparency and diffusivity of oxidized PDMS sheets is due to the mixed effect of the light-diffracting wrinkles and light-scattering cracks that dynamically form and disappear optically by stretching and releasing.

In order to probe the effect of applied strain on the ordering and patterning of wrinkles, we examined the diffraction patterns of incident light passing through the wrinkled PDMS sheets. Figure 4 shows the white light and monochromatic light (654 nm) diffraction patterns generated by a type A

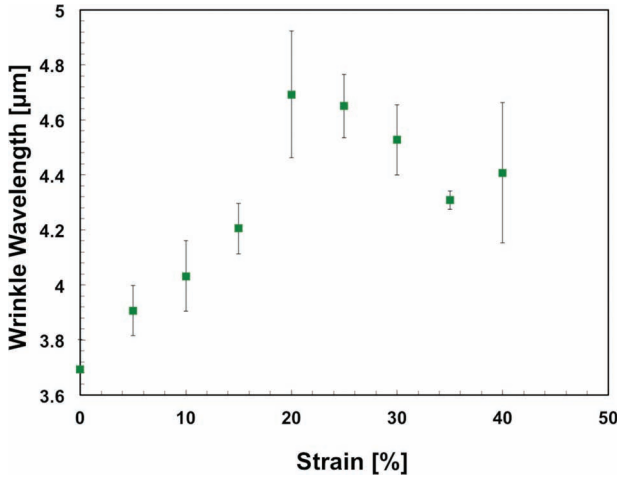

Figure 3. The evolution of the wrinkle wavelength of a type A sample with 20% pre-stretch as a function of applied strain.

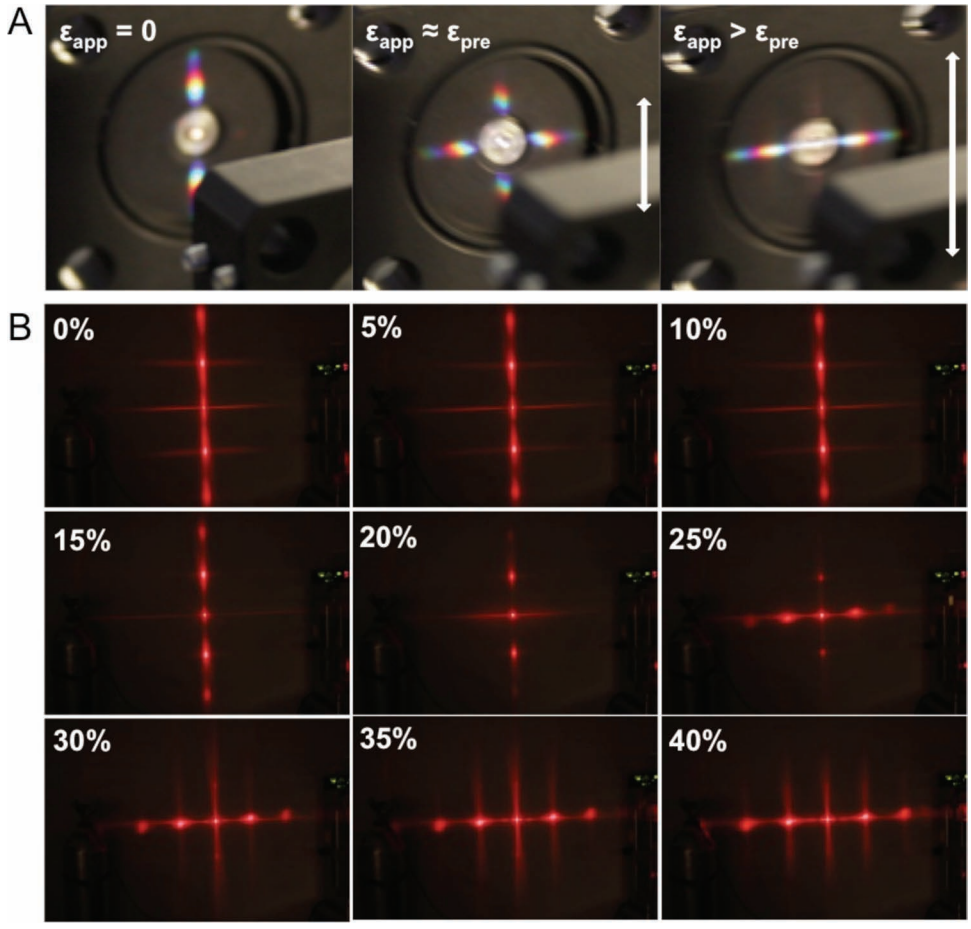

Figure 4. Photographs of white light diffraction (A) and monochromatic light diffraction (B) through a type A wrinkled PDMS sample prepared with 20% pre-stretching showing the switching of the orientation of the wrinkles. Numbers in (B) indicate applied strain relative to the initial length of the PDMS sheet. The horizontal line spread in the first image and the vertical spread in the last image in (B) are signatures of the cracks.

sample prepared with 20% pre-stretching under various applied strain values. Initially, typical blue to red spectral band (white light diffraction) or high intensity spots (monochromatic light diffraction) of increasing positive and negative orders from the center are oriented parallel to the axis of pre-stretching. The orientation of the diffraction pattern indicates that the wrinkles are initially oriented perpendicular to the axis of pre-stretching. Stretching a type A sample along the axis of pre-stretching gradually brings the diffraction spots closer and decreases the intensity until it is stretched to its initial length when oxygen plasma was introduced to create the stiff skin layer. These changes indicate that stretching a type A sample increases the pitch and decreases the amplitude of the initially existing wrinkles (primary wrinkles). Continued stretching beyond the initial length induces a characteristic, unique switching of the orientation of the diffraction patterns by 90 degrees. We attribute this switching behavior to the compression perpendicular to the axis of stretching due to the large Poisson's ratio of PDMS exceeding the critical buckling strain, hence creating new wrinkles (secondary wrinkles) along the axis of stretching and orthogonally oriented to the primary wrinkles.

Neither a type B sample nor a PDMS sheet cast against a silicon master with a sinusoidal groove pattern exhibits the above-mentioned switching behavior (See Movies 1, 2, and 3 in the Supporting Information). This is because these samples do not have an applied pre-strain that can be released under a stretching experiment, and applied strain only increases the overall stress in the skin layer. Interestingly, the coexisting orthogonal diffraction pattern can be seen only over a very narrow range of applied strain that is close to the pre-strain value used for creating the stiff skin layer. Our new pre-stretching and re-stretching experimental system can effectively create a condition that brings the net applied strain on the stiff membrane to a very small value, which would not be straightforward to produce using a type B sample. We hereafter refer to this narrow range of applied strain that induces the switching of the diffraction patterns as a 'transition region'. From this observation, the wrinkle patterns in the transition region are expected to consist of combinations of ordered structures parallel and perpendicular to the

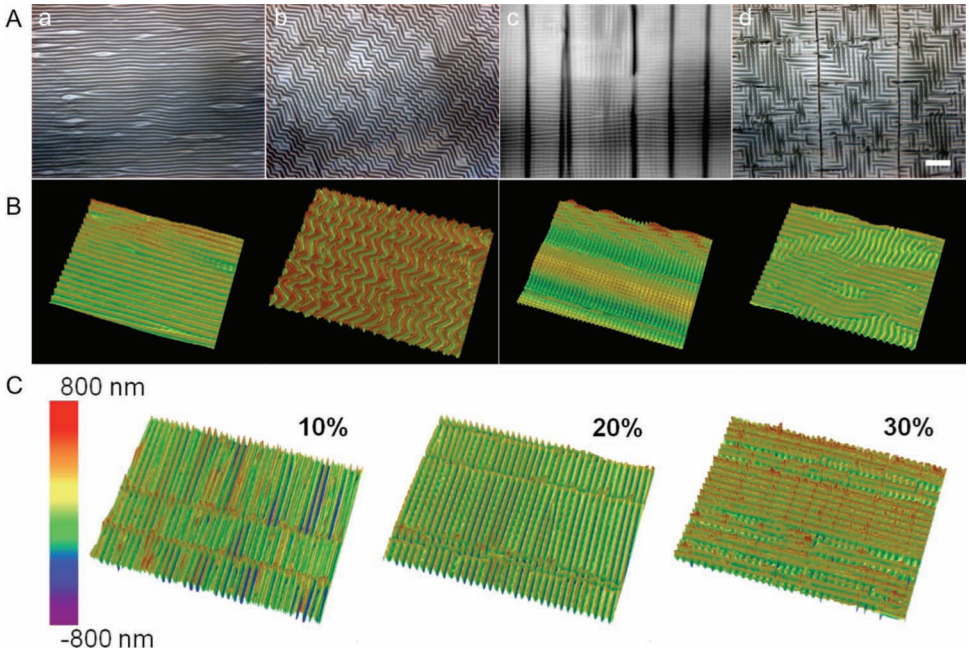

Figure 5. A,B) Optical microscopy images (scale bar = 20 μm) of various wrinkle patterns observed in stretching experiments and corresponding white light interference profilometry images. C) White light interference profilometry of a type A sample prepared with 20% pre-stretch under 10%, 20%, and 30% applied strains. All the white light interference profilometry images shown here represent a 118 μm × 90 μm rectangular area of each wrinkled surface. The rainbow color scale applies to both (B) and (C).

axis of stretching that give rise to vertical and horizontal diffraction patterns.

2.2. Strain-Dependent Evolution of Topographical Changes of Wrinkled PDMS near the Transition Region

To examine the detailed wrinkle patterns near the transition region, we characterized how the wrinkle patterns evolve as a function of applied strain using optical microscopy and white light interference profilometry. We also provide an analytical model to describe the interplay between applied mechanical strain and the strain from the residual stress in the film that allows us to observe various two-dimensional wrinkle patterns near the transition region (See Supporting Information). **Figure 5**A and B show the optical microscope images of all possible representative wrinkle patterns (stripes, herringbone, checkerboard, and labyrinth) observed in our experimental system and corresponding optical profilometry images, respectively. (i) The stripe pattern is observed either from a type A sample under applied strain values far from the pre-strain value or from a type B sample under a sufficiently large (>~5%) applied strain. (ii) The herringbone pattern is observed only from type B samples under relatively small deformation conditions, typically less than 5% of applied strain. (iii) The checkerboard pattern is observed only from a type A sample with applied strain values close to the pre-strain value and over a very narrow range (transition region). (iv) The labyrinth pattern is observed from both types of samples. In type A samples, it is predominantly observed near the transition region but only when the strain is released after the sample is overstretched beyond the pre-strain. This indicates that there is a hysteresis in strain-dependent wrinkle pattern formation. In type B samples, it is observed in the course of wrinkle patterns switching between herringbone patterns and quasi-ordered stripes and typically seen when the applied strain is slightly below the strain required for herringbone patterns.

From the surface profilometry data, we could extract information for the exact topography of the wrinkle patterns and their wavelength and amplitude under applied mechanical strain. When a pre-stretched sample is oxygen plasma-treated, there is pre-existing buckling pattern on the sample before removing the pre-stretch. After releasing the pre-stretch, large amplitude stripe patterns (primary wrinkles) are formed perpendicular to the pre-stretching orientation. During the very first stretching track for a freshly prepared type A sample, the amplitude of the primary wrinkles gradually decreases initially. When the applied strain is close to the initial pre-strain, the secondary wrinkles begin to develop on some areas where local strain is above the critical buckling strain. This creates checkerboard patterns only in some regions. When the sample is further stretched beyond the initial pre-stretching, the secondary wrinkles continue to form over the entire area of the surface. During the first releasing track of a type A sample, the amplitude of secondary wrinkles decreases but persists near the transition point. When the applied strain becomes close to the initial pre-strain again, the secondary wrinkles begin to abruptly switch to primary wrinkles forming predominantly labyrinth patterns followed by the formation of checkerboard patterns. In the second or later stretching tracks, checkerboard patterns

are more easily observed when crossing the transition region (See Movie 4 in the Supporting Information). This tendency is repeatedly observed from type A samples that had gone through at least one stretching-releasing cycle. We attribute the difference between the first stretching-releasing cycle and later cycles to the effect of crack formation. When a newly prepared type B sample is uni-axially stretched, the pre-existing quasi-ordered stripe patterns gradually evolve to small domains of labyrinth patterns then to a large number of labyrinth patterns with local herringbone patterns. With further stretching the stripes are re-oriented parallel to the axis of stretching. During the first releasing track of a type B sample, stripes abruptly turn their orientation to form small domains of labyrinth patterns (See Supporting Figure S2).

Figure 5C shows the surface topography of a type A sample (prepared with 20% pre-stretching) measured at various applied strain values, which clearly shows that a checkerboard pattern is formed near the transition region. To our knowledge, this is the first experimental observation of a checkerboard pattern, predicted to exist over a very narrow range of uniform membrane strain, purely based on the control of very small membrane strain. Interestingly, similar checkerboard type bi-directional wrinkle patterns have been found on the elytra of sap feeding beetle (Nitidulidae), *Pallodes*, exhibiting double spectral reflectance under white light illumination.[7] We attribute the formation of checkerboard pattern in our wrinkle-forming experiments to the balance between vanishingly small applied mechanical strain and the residual strain originated from the thermal strain due to temperature change and from the intrinsic strain from the formation of the oxidized layer. None of our experimental results up to 40% of pre-stretching indicated the formation of localized ridge wrinkling or folding possibly due to the high stiffness and brittleness of the oxidized layer.[15–17]

The crack formation upon stretching of oxidized PDMS can also be well studied by optical microscopy using our stretching experimental scheme. Very long cracks parallel to the axis of pre-stretching already develop as soon as the tension on a type A sample is released after oxygen plasma. This is because the PDMS substrate expands perpendicular to the axis of pre-stretching when the pre-strain is removed and puts the film under tension. When a newly prepared type A sample is stretched for the first time, these long cracks orthogonal to the primary wrinkles are optically visible up to the point where the applied strain is slightly beyond the pre-strain value. When the sample is overstretched beyond the fracture strength, new cracks (short cracks) parallel to the primary wrinkles develop within the long rectangular segments defined by existing long cracks. Therefore these short cracks are confined in between existing long cracks and divide the long segments into small rectangular segments of a finite aspect ratio. Since the stiff membrane is now separated into many small rectangular segments, the abrupt switching from secondary wrinkles to primary wrinkles during the releasing track always happens within each rectangular segment predominantly creating labyrinth patterns and continues until most of the secondary wrinkles are switched to primary wrinkles. It is obvious that these cracks act as a mechanism to release stress, thus the stress in a region adjacent to the crack with a size comparable to the film thickness is preferentially released. We note that stripe pattern wrinkles can only develop along the direction perpendicular to the cracks, while other two-dimensional wrinkles (e.g. labyrinth, checkerboard) are developed in the region far from the cracks as shown in Figure 5A-d. As the cracks develop, large shear stress is built along the interface between the film and the PDMS substrate in the vicinity of the cracks. After several stretching cycles, the film debonds from the substrate near the cracks and no wrinkles appear in these regions (See Supporting Information Figure S3).[18]

In the case of type B samples, only long cracks perpendicular to the axis of stretching can form, which separate the surface into rectangular segments of practically an infinite aspect ratio. On the releasing track, the stripes dynamically switch back to labyrinth pattern and local herringbone patterns, but are not confined inside a rectangular region defined by cracks as there is no short crack. When the strain is fully removed, the open cracks effectively disappear leaving only pinched cracks on the surface.

2.3. Implications and Potential Applications

Elastomeric substrates with surface nanostructures fabricated via controlled wrinkling have recently been used for tunable gratings,[19,20] guided self-assembly of particles and cells,[21,22] manipulation of proteins in nanofluidic devices,[23] reversible wetting surfaces,[24] anisotropic wetting surfaces,[25] dry adhesives,[26,27] and as a platform for measuring thin film mechanical properties.[1,28,29] With better control of the different achievable structures in this type of material system, one expects that these applications can be further optimized or evolved into additional concepts.

Based on the optical response to applied strain of the materials system reported above, we propose that the reproduction of this treatment on large area substrates presents potential alternatives to current smart window technologies, where the opacity of the structure is controlled via external stimuli. Unlike electrochromic windows that are triggered by an applied voltage, these wrinkled elastomers can be switched mechanically to reversibly and instantaneously control the amount of transmitted light ("mechanochromic" window) into an area by simple mechanical deformation of the material. This system not only can provide a means to adaptive shading, but also function as a switchable privacy screen as demonstrated in **Figure 6**A. Furthermore, by using a shadow mask during plasma treatment, a type of encryption can be established where messages or graphics can be reversibly revealed and concealed upon stretching and releasing the material as shown in Figure 6B, C, and Movie 5 in the Supporting Information. The narrow width of the wrinkle-switching transition region can also potentially utilized to develop an ultrasensitive strain sensor that transduces compressive or tensile strain into changes in diffraction patterns.

3. Conclusion

We have demonstrated an experimental system in which pre-stretched and oxygen plasma-treated PDMS sheets can display

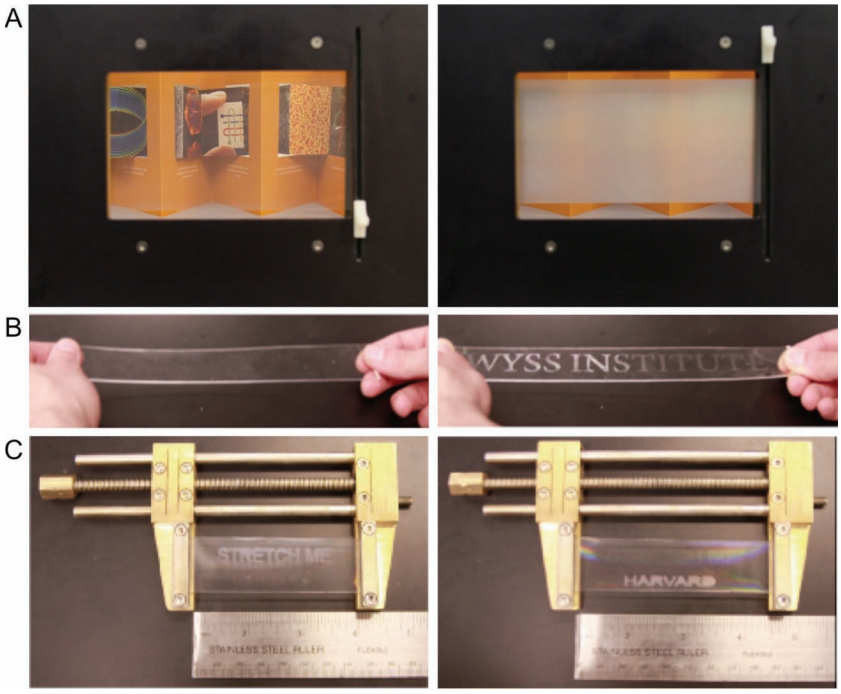

Figure 6. Photographs showing mechanically switched optical transparency of oxygen plasma-treated PDMS sheets. A) Transition between optically clear state (left, unstretched) and opaque state (right, stretched) observed from a type B sample mounted inside a black metal frame with a slider that stretches the PDMS sheet. B) Type B sample prepared with a shadow mask revealing the letter "WYSS INSTITUTE" when stretched. C) Mixed effect from type A treatment at the top half and type B treatment at the bottom half. With no stretching, the sample displays a message "STRETCH ME". When the sample is stretched to its initial length for oxygen plasma treatment, the initially visible message disappears but a new message "HARVARD" appears. When the sample is overstretched, both messages are visible (picture not shown). All of these effects disappear when the PDMS sheet is fully submerged in a high refractive index liquid (e.g. water) due to index matching.

various two-dimensional buckling patterns under precisely and predictably controlled bi-axial strains. In the course of pre-stretching, oxidizing, and re-stretching experiment, persistent stripe wrinkle patterns and transient two-dimensional wrinkle patterns emerge from the interplay between applied mechanical stress and residual stress in the thin oxidized PDMS membrane. Our new experimental system allowed the observation of a transition region in which orthogonally oriented wrinkles coexist, forming checkerboard and labyrinth patterns. Through this transition region, stripe pattern wrinkles uniquely switch their orientations. These dynamically evolving wrinkles cause the switching of diffraction patterns and the changes in the diffraction efficiency contributing to the macroscopic switching of the optical transparency of oxygen plasma-treated PDMS sheets. We have shown a simple analytical model accounting for the residual stress in the membrane that explains the coexistence of longitudinal and transverse wrinkles. These wrinkled PDMS sheets with predictable macroscopic optical properties can be used as instantaneous switchable privacy screens or encryption of messages and graphics that reversibly appear and disappear by simply stretching them. The buckling problem in the presence of orthogonally oriented one-dimensional wrinkles and the detailed mechanism and the evolution from one-dimensional wrinkle patterns to two-dimensional wrinkle patterns remain as interesting problems that deserve further study.

4. Experimental Section

A two-part silicone elastomer (DOW Sylgard 184) was mixed in a 10:1 mass ratio of base to curing agent. A dual centrifuge mixer was used to create a uniform mixture of the two components. Once thoroughly mixed, the material was degassed for a period of 30 min to remove any trapped air bubbles. After degassing, the mixture was poured into a flat, shallow dish and placed into an oven at 60 °C to cure over a period of 2 hours. Once cured, the elastomer sheet is peeled away from the dish.

The elastomer sheet can then be easily cut into various shapes and sizes, depending on the application. For the plasma treatment process, the sheets were kept to thicknesses ranging from 0.5–2.5 mm. Prior to plasma treatment, the elastomeric samples were clamped into a uni-axial, screw-driven stretching device and then stretched to the desired pre-stretch state (0%–50%). Once prepared, the stretched sample is placed into the plasma vacuum chamber. Once the chamber is evacuated (2 min), oxygen gas is introduced to the system at 10 sccm for 1 min, at which point the gas is turned off and the vacuum pump is allowed to reduce the pressure in the system (30 s). A 40 kHz power source at 100 W was used to ionize the oxygen gas. The elastomer is placed at an approximate distance of 8 cm from the electrode. Treatment times can depend on a variety of parameters, but were optimized for optical properties (70 s). After the plasma treatment, the chamber is vented to atmospheric pressure and the strain is slowly released from the sample.

For optical characterization, 75 mm x 25 mm rectangular test strips were prepared. After oxygen plasma treatment, the samples were mounted back onto the stretching device. A tungsten lamp (Model LS-1-LL, Ocean Optics) was coupled through a 400 µm diameter fiber-optic cable to an optical setup. An incident light collimated through a 25 mm collimating lens to approximately a 1 cm diameter circular beam was passed through a PDMS sample at normal incidence. The transmitted light was collected and focused onto a second fiber optic cable using a 50 mm diameter collection lens with a focal length of 60 mm placed 7 cm behind the PDMS sample. In the collimated beam path, an adjustable aperture was used to control the illuminated area on the sample. A custom software controlled spectrometer (Model USB2000+ VIS-NIR, Ocean Optics) was used to collect and process the optical signal. Transmittance spectra (400–900 nm, 25 ms integration) were collected for each sample as a function of uni-axial strain with 2.5% incremental steps. The background spectrum was collected without turning on the light source and all the spectra collected were normalized by a spectrum collected without placing a sample in the beam path.

The surface structure imparted by the elongation and compression of the second material formed on the substrate was examined with white light optical profilometry (Model NT-1100, Veeco). Measurements were taken in VSI mode with a 50× objective lens and a modulation threshold of 0.5%. The raw data was tilt corrected and smoothed with a low pass filter.

The intrinsic stress induced on the PDMS by the plasma oxidation process was estimated using thin film stress measurements (TOHO Technology FLX-2320-S) on a 4 inch silicon wafer with a 25 um thick spin coated layer of PDMS. The curvature was measured at 25 °C, across

the entire wafer width along the 0°, 30°, 60°, and 90° directions after the PDMS was cured and again after the plasma oxidation step.

Supporting Information

Supporting Information is available from the Wiley Online Library or from the author.

Acknowledgements

This work was supported by U.S. AFOSR Multidisciplinary University Research Initiative under award number FA9550–09–1–0669-DOD35CAP. Part of this work was performed at the Center for Nanoscale Systems (CNS) at Harvard University supported by the NSF under award no. ECS-0335765. We thank Prof. John Hutchinson for discussions of the theoretical explanations, Chuck Hoberman for discussions of the applications of wrinkled PDMS, and Dr. Alison Grinthal for the critical comments on the manuscript. We thank Tom Blough for the design and fabrication of customized stretching devices and frames and Dr. James C. Weaver for the graphical illustrations of wrinkled PDMS sheets.

Received: October 2, 2012
Published online: April 12, 2013

[1] J. Y. Chung, A. J. Nolte, C. M. Stafford, *Adv. Mater.* **2011**, *23*, 349.
[2] S. Yang, K. Khare, P.-C. Lin, *Adv. Funct. Mater.* **2010**, *20*, 2550.
[3] A. Schweikart, A. Horn, A. Böker, A. Fery, *Adv. Polym. Sci.* **2010**, *227*, 75.
[4] Y. Mei, S. Kiravittaya, S. Harazim, O. G. Schmidt, *Mater. Sci. Engin. R* **2010**, *70*, 209.
[5] P.-C. Lin, S. Vajpayee, A. Jagota, C.-Y. Hui, S. Yang, *Soft Matter* **2008**, *4*, 1830.
[6] G. F. Sun, J. F. Jia, Q. K. Xue, L. Li, *Nanotechnology* **2009**, *20*, 355701.
[7] A. E. Seago, P. Brady, J.-P. Vigneron, T. D. Schultz, *J. Royal Soc. Interface* **2009**, *6*, S165.
[8] H. M. Whitney, B. J. Glover, R. Walker, A. G. Ellis, *Curtis's Botanical Magazine* **2011**, *28*, 349.
[9] R. T. Hanlon, C.-C. Chiao, L. M. Mäthger, A. Barbosa, K. C. Buresch, C. Chubb, *Phil. Trans. Roy. Soc. B* **2009**, *364*, 429.
[10] X. Chen, J. W. Hutchinson, *J. Appl. Mech.* **2004**, *71*, 597.
[11] Z. Y. Huang, W. Hong, Z. Suo, *J. Mech. Phys. Solids* **2005**, *53*, 2101.
[12] D.-H. Kim, N. Lu, R. Ma, Y.-S. Kim, R.-H. Kim, S. Wang, J. Wu, S. M. Won, H. Tao, A. Islam, K. J. Yu, T.-i. Kim, R. Chowdhury, M. Ying, L. Xu, M. Li, H.-J. Chung, H. Keum, M. McCormick, P. Liu, Y.-W. Zhang, F. G. Omenetto, Y. Huang, T. Coleman, J. A. Rogers, *Science* **2011**, *333*, 838.
[13] F. Ilievski, A. D. Mazzeo, R. F. Shepherd, X. Chen, G. M. Whitesides, *Angew. Chem. Int. Ed.* **2011**, *50*, 1890.
[14] H. G. Allen, *Analysis and Design of Structural Sandwich Panels*-Franklin Book Co., Oxford, UK **1969**.
[15] K. Efimenko, M. Rackaitis, E. manias, A. Vaziri, L. Mahadevan, J. Genzer, *Nat. Mater.* **2005**, *4*, 293.
[16] L. Pocivavsek, R. Dellsy, A. Kern, S. Johnson, B. Lin, K. Y. C. Lee, E. Cerda, *Science* **2008**, *320*, 912.
[17] J. Zang, X. Zhao, Y. Cao, J. W. Hutchinson, *J. Mech. Phys. Solids* **2012**, *60*, 1265.
[18] N. Bowden, S. Brittain, A. G. Evans, J. W. Hutchinson, G. M. Whitesides, *Nature* **1998**, *393*, 146.
[19] C. Harrison, C. M. Stafford, W. Zhang, A. Karim, *Appl. Phys. Lett.* **2004**, *85*, 4016.
[20] C. Yu, K. O'Brien, Y.-H. Zhang, H. Yu, H. Jiang, *Appl. Phys. Lett.* **2010**, *96*, 041111.
[21] S. Hiltl, M.-P. Schürings, A. Balaceanu, V. Mayorga, C. Liedel, A. Pich, A. Böker, *Soft Matter* **2011**, *7*, 8231.
[22] X. Jiang, S. Takayama, X. Qian, E. Ostuni, H. Wu, N. Bowden, P. Le Duc, D. E. Ingber, G. M. Whitesides, *Langmuir* **2002**, *18*, 3273.
[23] S. Chung, J. H. Lee, M.-W. Moon, J. Han, R. D. Kamm,*Adv. Mater.* **2008**, *20*, 3010.
[24] S. G. Lee, D. Y. Lee, H. S. Lim, D. H. Lee, S. Lee, K. Cho, *Adv. Mater.* **2010**, *22*, 5013.
[25] J. Y. Chung, J. P. Youngblood, C. M. Stafford, *Soft Matter* **2007**, *3*, 1163.
[26] H. E. Jeong, M. K. Kwak, K. Y. Suh, *Langmuir* **2010**, *26*, 2223.
[27] E. P. Chan, E. J. Smith, R. C. Hayward, A. J. Crosby, *Adv. Mater.* **2008**, *20*, 711.
[28] C. M. Stafford, C. Harrison, K. L. Beers, A. Karim, E. J. Amis, M. R. Vanlandingham, H.-C. Kim, W. Volksen, R. D. Miller, E. E. Simonyi, *Nat. Mater.* **2004**, *3*, 545.
[29] J. Y. Chung, J.-H. Lee, K. L. Beers, C. M. Stafford, *Nano Lett.* **2011**, *11*, 3361.